Solid-State Structures

DOI: 10.1002/anie.201203775

Two-Dimensional Antiferromagnetism in the $[Mn_{3+x}O_7][Bi_4O_{4.5-y}]$ Compound with a Maple-Leaf Lattice**

*Almaz Aliev, Marielle Huvé, Silviu Colis, Marie Colmont, Aziz Dinia, and Olivier Mentré**

Oxides with two-dimensional (2D) configurations between metal centers have been intensively studied and still remain a hot topic in the field of materials chemistry because they can lead to a variety of behaviors, such as superconductivity,[1] low-dimensional magnetism and frustration,[2] or more generally any kind of 2D confined properties. Besides the understanding of the physics involved, novel potential applications make the concerned materials of high interest at several levels, taking into account the stacking between different 2D units bringing their own specificities. For instance, $Ca_3Co_4O_9$ derivatives ($[CoO_2][Ca_2CoO_{3-\delta}]_{0.62}$), apart from thermoelectric properties, can be seen as the stacking of electronic conducting $[CoO_2]$ CdI_2-like layers and anionic-conducting $[Ca_2CoO_{3-\delta}]$ rock-salt layers, which offer good performance for mixed electronic–ionic conductors for solid-oxide fuel-cell applications.[3,4] Other relevant examples concern spintronics specificities in which heterostructures made of magnetic/nonmagnetic units control the field-dependent transport, such as in the spin-valve effect (SVE).[5] Bulk-SVE for Cr-doped $Ca_3Ru_2O_7$ with disconnected ferromagnetic (FM) double slabs[6] and spin–flop transition between disconnected FM-blocks in barium cobalt oxohalides has recently been reported.[7] Nowadays, the primary challenge is the discovery of novel compounds built on the stacking of elementary units that are disconnected as much as possible. For enhanced transport and magnetic properties inherent to their 2D character, metal networks based on triangular lattices are particularly pertinent owing to short M–M separations and high connectivity. Herein, we present the preparation, crystal structure, and primary characterization of $Bi_4Mn_3O_{11.5}$, which could be described as a $[Mn_{3+x}O_7]$ $[Bi_4O_{4.5-y}]$ intergrowth. Besides the striking presence of truly disconnected antiferromagnetic layers, it is an extremely rare realization of a maple-leaf lattice (1/7-depleted triangular lattice) of octahedral edge-sharing $Mn^{3+/4+}$ ions.[8] The main characteristics of several well-known octahedral 2D lattices[9] related to the parent triangular lattice by incremental depletion are shown in the Figure 1. The 1/7 depletion is intermediate between the triangular and honeycomb lattices.

A black triangular-like platelet was selected for single-crystal XRD analysis (see the Experimental Section). The structure corresponds to the intergrowth between to subunits stacked along the *c* axis (Figure 2a). Besides the ideal framework of formula $Bi_4Mn_3O_{11.5}$, clues for disorder have been located by analyzing the residual electronic density maxima in both the two stacked sublattices.

The $[Bi_4O_{4.5-y}]$ sublattice contains three independent oxygen atoms (O1, O2, O6) and two bismuth atoms (Bi1,

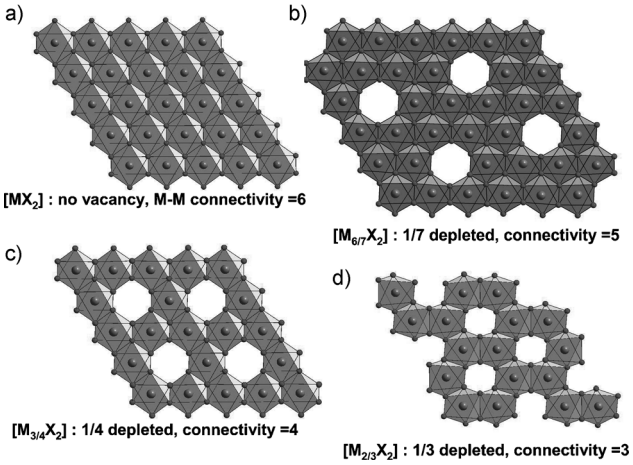

Figure 1. Projection and characteristics of 2D octahedral layers of a a) triangular lattice, b) maple-leaf lattice, c) honeycomb lattice, and d) Kagomé lattice.

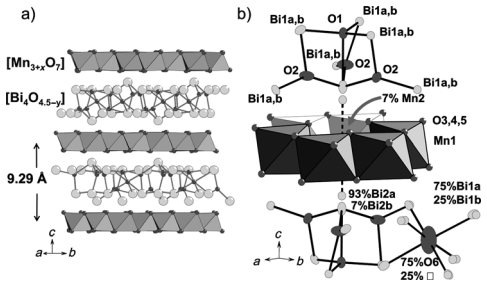

Figure 2. a) View of the $[Mn_{3+x}O_7][Bi_4O_{4.5-y}]$ intergrowth. b) Detail of O–Bi connection at the apex of a void.

[*] A. Aliev, Prof. M. Huvé, Dr. M. Colmont, Dr. O. Mentré
Université Lille Nord de France, CNRS UMR8181, Unité de Catalyse et de Chimie du Solide, UCCS USTL
59655 Villeneuve d'Ascq (France)
E-mail: olivier.mentre@ensc-lille.fr
Dr. S. Colis, Prof. A. Dinia
Institut de Physique et Chimie des Matériaux de Strasbourg (IPCMS), UMR 7504 UDS-CNRS (UDS-ECPM)
23 rue du Loess, BP 43, 67034 Strasbourg Cedex 2 (France)

[**] The authors thank the CNRS, French Ministry of Research and High Education, and Région Nord-Pas-de-Calais for the funding of diffractometers. This work was carried out under the framework of the MAD-BLAST project supported by the ANR (Grant ANR-09-BLAN-0187-01). We also thank Dr. E. Janod, (IMN, Nantes, France) for fruitful discussions.

Supporting information for this article is available on the WWW under http://dx.doi.org/10.1002/anie.201203775.

Bi2) arranged in a complex manner. Because of the Bi^{3+} lone pair, the oxygen coordination around central bismuth is generally very irregular. By itself, such coordination justifies the intensive use of an oxo-centered polyhedra approach in Bi-based oxides and salts.[12] This concept allows the structural relationship to be made between the various Bi_2O_3 polymorphs.[13] It follows that both O1 and O2 occupy the centers of OBi_3 triangles (2.08 Å < O–Bi < 2.51 Å). For O1, this coordination is completed by an apical Bi1 atom towards the $[Mn_3O_7]$ module; O6 is at the center of a regular OBi_6 octahedron. The latter atom is characterized by strongly anisotropic thermal parameters, and its refined occupancy converged to about 75%. Similarly, owing to strong satellite peaks on Fourier difference maps, Bi1 was split over two close positions (Bi1a (ca. 75%) and Bi1b (ca. 25%)), which indicates the coexistence of 3/4 of OBi_6 octahedra (d(O6–Bi1a) = 2.646(1) Å) and 1/4 of $\square Bi_6$ octahedra (d(□–Bi1b) = 2.727(7) Å). It yields the formula $[Bi_4O_{4.5-y}]$, with $y = 0.15$. The Bi1 split locally affects both O1 and O2 coordination. Bi2 was also split over two positions aligned along c, owing to high residual electronic density: Bi2a(93%) and Bi2b(7%) (Figure 2b). This disorder is related to an outstanding disorder occurring in the next building units detailed below.

The $[Mn_{3+x}O_7]$ sublattice is composed of three oxygen (O3, O4, O5) and two manganese (Mn1, Mn2) independent crystallographic positions. The ideal lattice of formula Mn_3O_7 creates voids, of which about 7% are occupied by the interstitial Mn2. It follows that, depending on the absence or presence of Mn2 in these cavities, Bi2 occupies either Bi2a or Bi2b within the next subunits (7% d(Mn2-Bi2a) = 3.082(4) Å versus 93% d(□–Bi2b) = 2.415(1) Å), with respect to strong Bi–Mn electrostatic repulsion. The refined occupancy leads to the formula $[Mn_{3+x}O_7]$ with $x = 0.03$.

Owing to the local disorder observed on several sites, single crystals were cooled down in situ to 100 K. The evolution of the lattice parameters upon cooling is given on the Figure 3. In addition to the thermal lattice contraction, a sharp event is observed around $T_t = 240$ K. Both a and c are exaggeratedly shortened below this order–disorder transition. The crystal structure was then collected and refined at 100 K (Table 1; Supporting Information, S1). The crystal structure remains essentially unchanged, while Bi1 does not show any more clues for a split and O6 is displaced from its central 3(b) site (1/2, 2/3, 1/6) into a 6(c) site (1/3, 2/3, $z = 0.176(1)$) but conserves a partial occupancy. Then below 240 K, $O6Bi1_6$ is characterized by 3 × O6–Bi1 = 2.545(2) Å and 3 × O6–Bi1 = 2.796(2) Å. The transition does not affect the Bi2a/Bi2b split, which corresponds with the partial occupancy of the voids by Mn2. However, below T_t, the changes in the interatomic distances affect magnetic and transport properties, as discussed below.

Layered manganese oxides are often associated to the phyllomanganate minerals, such as lithiophorite, rancieite, and takanelite.[8] More generally, the structural type birnessite[14] (layered type triangular MnO_2, separated by alkali and alkaline earth metal and water molecules), is described as the most representative type. In the parent compound, even if the ideal $[Mn_3O_7]$ array is related to such network, its main specificity results in the ordering of the 1/7th vacancies (Figure 1b). The occurrence of random vacancies in the birnessite was investigated, as trace metals such as Zn appear to be located at their vertices by sorption in birnessite minerals found in soils, aquifers, streams, and wetlands.[15,16] To our knowledge, a regular 1/7-depleted Mn triangular

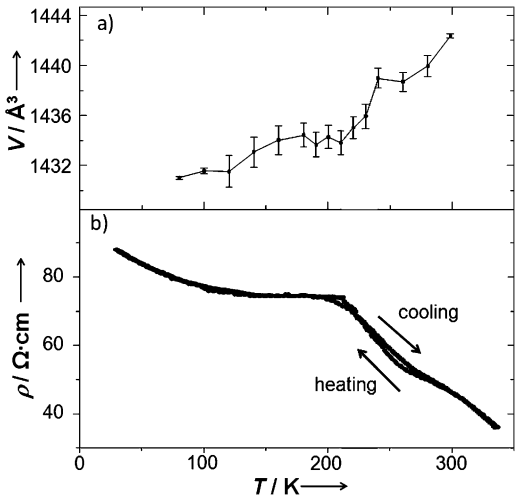

Figure 3. Evidence of a transition below 240 K as a) a lattice volume contraction from single-crystal XRD; and b) an anomaly on the electric four-probe resistivity measurement on a single crystal.

Table 1: Selected distances in $Bi_4Mn_3O_{11.5}$ at both sides of the order–disorder transition.

100 K			293 K		
		d [Å]			d [Å]
Bi1	O1	2.1868(7)	Bi1a/ Bi1b	O1	2.146(3)/ 2.318(3)
	O2	2.115(5)		O2	2.134(4)/ 2.099(4)
	O2	2.255(5)		O2	2.283(3)/ 2.247(3)
	O3	2.887(5)		O3	2.886(3)/ 2.918(4)
	O5	2.532(4)		O5	2.511(3)/ 2.611(3)
	O6/ O6′	2.80(2)/2.54(2)		O6	2.708(2)/ 2.522(2)
Bi2a Bi2b	O1	3.355(7)/ 2.675(9)	Bi2a/ Bi2b	O1	3.351(4)/ 2.685(5)
	O2 × 3	2.518(7)/ 2.213(8)		O2 × 3	2.489(4)/ 2.191(5)
	O3 × 3	2.246(5)/ 2.705(7)		O3 × 3	2.259(3)/ 2.707(4)
Mn1	O3	1.900(5)	Mn1	O3	1.906(3)
	O3	1.941(5)		O3	1.937(3)
	O4	1.965(3)		O4	1.961(2)
	O5	1.921(5)		O5	1.921(3)
	O5	2.059(4)		O5	2.059(2)
	O5	1.936(6)		O5	1.943(3)
Mn2	O3 × 6	2.107(6)	Mn2	O3 × 6	2.119(3)
Mn1	Mn1 × 2	2.9490(17)	Mn1	Mn1 × 2	2.9540(8)
	Mn1	3.0107(12)		Mn1	3.0166(6)
	Mn1 × 2	2.8732(18)		Mn1 × 2	2.8763(8)
	Mn2	2.8729(8)		Mn2	2.8761(3)

lattice was only observed in a related mineral, the chalcophanite $[ZnMn_3O_7{\cdot}3H_2O]$,[8] which has not yet been investigated for its physical properties. This particular topology corresponds to the fourth of the eleven Archimedean tilings (T_4), which is also called the maple-leaf lattice.[9,17] Topologies T_i ($i=1$ to 11) represent the prototypes of 2D arrangements of regular polygons, which are particularly interesting for low-dimensional magnetism, where 2D (spin) lattices are obtained by considering spins on each vertices connecting neighboring polygons. More precisely, the T4 maple-leaf topology (1/7-depleted, M–M connectivity = 5) is rare[18,19] and corresponds to the intermediate between the well-known honeycomb lattice (1/3-depleted, connectivity = 4) and the parent triangular lattice (non-depleted, connectivity = 6). The correspondence between such lattices made of edge-sharing octahedra is shown on the Figure 1, which also shows the Kagomé lattice (1/4-depleted, connectivity = 4). According to the ideal formula of the structure $Bi_4Mn_3O_{11.5}$, without taking into account neither the O6 vacancies nor the interstitial Mn2, the mean Mn valence on the maple-leaf lattice is $Mn^{+3.66}$. For interstial Mn sites, the Mn2–O bonds are 2.12 Å, which suggest a Mn^{2+} valence (see bond valence sum calculation in the Supporting Information, S2.1) while Mn1 (mean Mn1-O = 1.96 Å) is consistent mixed $Mn^{3+/4+}$ valence. Then, after consideration of the defects, the $Bi_4Mn^{+3.54}Mn^{+2}{}_{0.03}O_{11.35}$ formula pictures at best the reduction of octahedral Mn species from $Mn^{+3.66}$ to $Mn^{+3.5}$ by both incorporation of interstitial Mn^{2+} cations and creation of oxygen vacancies. The defects have been systematically detected in similar proportion on several collected single crystals. This is in good agreement with the mean Mn oxidation state of 3.43(3) titrated by iodometry on the single-phase polycrystalline sample (described below).

The striking disproportionation into distinct Mn valences in neighboring crystallographic sites (Mn^{2+} interstitial defects versus $Mn^{3+/4+}$ network cations), even if rare, is not unique. For instance in several hexagonal perovskites such as $Ba_7Mn^{3+/4+}{}_3Mn^{5+}{}_2Ca_2O_{20}$,[20] Mn^{5+} occupies tetrahedra separated from $Mn^{3+/4+}$ strings of face-sharing octahedra by Ca^{2+} cations. Closer to our compound, a direct connection between ordered Mn^{2+} and Mn^{4+} octahedra was pointed out in $Pb_3Mn^{4+}{}_3Mn^{2+}{}_2V_2O_{16}$.[21] In this compound, the mean Mn–O distances around both species ($d(Mn^{4+}{-}O) = 1.93$ Å, $d(Mn^{3+}{-}O) = 2.15$ Å) are very similar to Mn coordination found in $[Mn_{3+x}O_7][Bi_4O_{4.5-y}]$, which comfirm our assignment of oxidation numbers. Even if only present as minor defects, it could explain the difficulties encountered to prepare single-phase materials. Indeed, some aspects about the synthesis of single-phase powder materials deserve extra detail in addition to the major points given in the Experimental Section. In fact, using the stoichiometry deduced from the structure determination, only the heating at medium temperature (ca. 773 K) of a well-dispersed Bi/Mn/O mixture by the Pechini method allows for the preparation of the target sample. At higher temperature $Bi_2Mn^{3.5+}{}_4O_{10}$ becomes predominant under all tested atmospheres (air, N_2, Ar, O_2), which shows that the stabilization of mixed Mn^{2+}–$Mn^{3+/4+}$ valence is essentially governed by the thermal treatment. Figure 4 a–e shows XRD results after various synthesis methods. The main difference

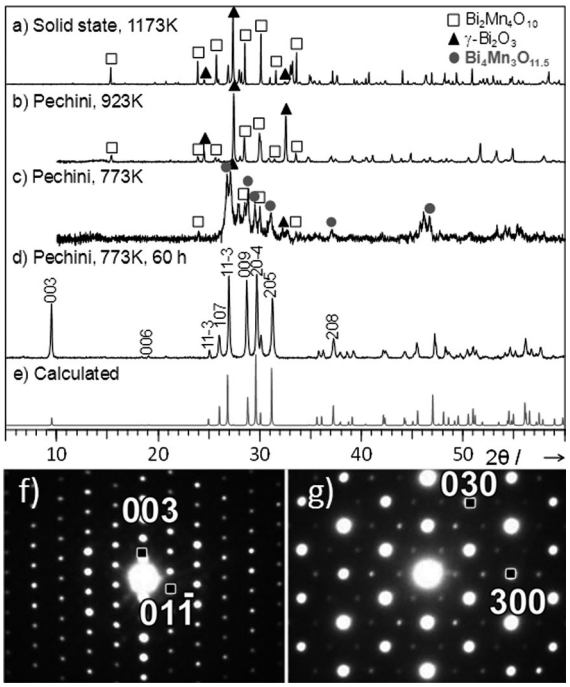

Figure 4. Comparison of a)–d) experimental XRD and e) calculated patterns after different stages of synthesis. In (b) and (c) the residue from the Pechini method was decomposed in situ in the diffractometer. d) The powder ED patterns: f) systematic [100] and g) particular [001] zone axes, with evidence of primitive spots (rare case) in the latter.

between single-crystal and powder compounds are a somewhat longer c parameter for the latter ($a = 7.7013(6)$ Å, $c = 28.007(2)$ Å). It may suggest a more important concentration of defects in both sublattices, and thus the need for interstitial Mn^{2+} in the maple-leaf voids to stabilize the phase.

It is striking that area-selected electronic diffraction patterns mostly correspond to the R-lattice conditions ($-h+k+l=3n$), but sometimes extra spots are observed after long-time acquisition. The supercell dataset is indexed in a primitive cell with same lattice parameters, but was only observed on the [001] zone axis patterns. It indicates that the defects mentioned above would (partially) order within (a, b) planes, while no correlations are observed between stacked individual modules. Precession frames calculated from the single-crystal XRD collection does not show evidence of similar effects, which indicate that it concerns micrometric or smaller domains but is lost at the single crystal scale (> 250 μm in average). In the scope of this paper it appears ambitious to argue about the structural origin of such local orderings. However, we can suggest that the weak extra intensities play in favor of oxygen ordering in the $[Bi_4O_{4.5-y}]$ sublattice rather than Mn^{2+} in the $[Mn_{3+x}O_7]$ voids, this latter being directly in connection with the Bi2a/Bi2b organization on two well-separated positions.

The resistivity versus temperature was measured on a single crystal using the four probes method (Figure 2 b). Owing to the small size of available crystals, contacts were

placed such that both $\rho(a, b)$ and $\rho(c)$ contribute to our experimental data. However, in such a 2D crystal structure, the electronic transport is favored in-plane, following mixed valence Mn paths. The lattice contraction observed below $T_t = 240$ K is accompanied by a change of $\rho(T)$ such that the resistivity is less temperature-dependent below T_t. Efforts to grow larger well-shaped single crystals are currently underway, thereby aiming for a more clear picture of the anisotropy of the transport properties.

The parent compound is the first synthetic oxide that realizes a true 2D 1/7-depleted triangular lattice. The mixed Mn^{3+} (d^4, $S=2$) and Mn^{4+} (d^3, $S=3/2$) valence is of high importance at both the experimental and theoretical level. To our knowledge, apart from the chalcophanite[8] mineral, only two magnetic systems built on a maple-leaf lattice were reported, if only the arrangement between magnetic cations is considered: the organometallic complex $M_x[Fe(O_2CCH_2)_2NCH_2PO_3]_6{\cdot}n\,H_2O$,[19] in which the iron cations approximate this topology but are distant and lead to a paramagnetic behavior at all temperature, and the mineral spangolite $Cu_6Al(SO_4)(OH)_{12}Cl{\cdot}3\,H_2O$, in which Cu^{2+} cations form a maple-leaf lattice, but extended antiferromagnetic (AFM) exchanges are dominated by dimerization[18] (from a theoretical prediction intensively calculated and discussed for an $S=1/2$ Heisenberg antiferromagnet (HAFM) on a 1/7-depleted triangular lattice). Indeed, a well-established 2D magnetic long-range ordering (LRO)[22] is expected to survive strong quantum fluctuations present in such frustrated layer, however it would be strongly weakened.[17] The understanding of our mixed-valence Mn system deserves theoretical modeling, but predictions for HAFM are informative for preliminary interpretations. The thermal evolution of the susceptibility (approximated as M/H) and its inverse are presented in the Figure 5. Above 210 K it follows a Curie–Weiss law $\chi = C/(T-\theta)$ leading to $\theta = -184.6$ K and $\mu_{eff} = 7.78\ \mu_B$/f.u. This value is in excellent agreement with $\mu_{eff} = 7.65$ μB/f.u. calculated for 1.5 Mn^{3+}(S=2) and 1.5 Mn^{4+}(S=3/2) in a spin-only approximation, according to the charge distribution discussed above. Strong predominant AFM couplings, indicated by the high negative θ value, are responsible for the concave upward evolution of $\chi^{-1}(T)$ below the transition. This behavior, according to the important separation (> 9 Å) between the magnetic subunits, most certainly shows the setting of important 2D AFM correlations, resulting in extended frustrated domains, as described for $S=1/2$ HAFM 2D maple-leaf layers.[17] It appears obvious that the structural contraction evidenced below 240 K plays an important role on both the electric conductivity and the magnetic interactions. The magnetic paths between $Mn^{3+/4+}$ centers (given in the Supporting Information, S3) involve interatomic separation in the range 2.87 Å < $d_{(Mn-Mn)}$ < 3.01 Å associated with Mn-O-Mn angles of about 97°. According to Goodenough–Kanamori rules, super-exchanges between isovalent Mn^{3+} or Mn^{4+} species are expected, whereas neither ferromagnetic Mn^{3+}-O-Mn^{4+} double exchanges nor super-exchanges do not seem predominant in this compound. No obvious clues for a magnetic ordering were detected on further cooling down to 2 K. However, a weak anomaly was detected at 50 K that could sign a minor structural reorganization. The ZFC/FC divergence observed on $\chi(T)$ at 6 K is not yet clearly understood. It is not typical of 3D Néel ordering, but is reminiscent of what was observed on the birnessite-type layered MnO_{2-x} structure below 9.2 K.[23] As suggested for this structurally related compound, it could correspond to very weak spin canting or uncompensated spin structure, which in our case is likely to be associated to the interstitial Mn^{2+} defects. We note that at 1.8 K, M(H) shows a weak hysteresis opening that is not observed at 6 K (remanent moment = $7.10^{-3}\ \mu_B$/f.u.). Increasing the applied field, it is striking that M(H) linearly but reversibly increases up to 0.6 μ_B/f.u. at 7 T. This relatively high value, in the context of predominant AFM exchanges and frustrated spin arrangement, denotes a progressive spin reversal under increasing external field.

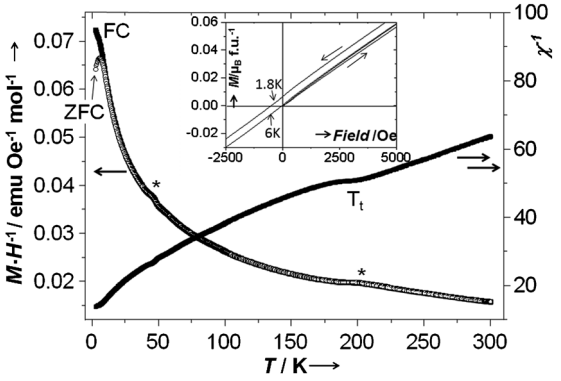

Figure 5. ZFC/FC plots of M/H versus temperature at 0.1 Tesla. * indicate magnetic anomalies. Inset: a portion of $M(H)$ at $T=6$ K and 1.8 K in μ_B/f.u.(Oe). It was measured up to 7 Tesla.

In conclusion, we have shown the preparation, crystal structure, and characterization of $[Mn_{3+x}O_7][Bi_4O_{4.5-y}]$, which is formed by the stacking of non-stoichiometric $[Bi_4O_{4.5-y}]$ blocks and $[Mn_{3+x}O_7]$ layers. Mixed-valence cations (approximately $Mn^{3.5+}$) form a rare example of maple-leaf 2D lattice by edge-sharing MnO_6 octahedra. About 7% of the open voids are randomly occupied by Mn^{2+} cations. In addition to minor structural ordering below 240 K, which strongly influences transport and magnetic properties, there are several indications of it being a true 2D antiferromagnet, which is in agreement with interlayer separation of about 9.3 Å. Besides the general interest in novel structural types, new frustrated magnetic topologies, and the unusual physics involved, $Bi_4Mn_3O_{11.5}$ offers several other potentialities as a result of its intergrowth 2D structure, for example, the prospection for cationic doping that is able to favor ferromagnetic layers for model spintronics applications. The potential mixed ionic/electronic conduction in well-separated subunits also appears promising, taking into account the well-known efficient O^{2-} transport of Bi-based oxides.[24]

Experimental Section

Single crystals of the title compound $Bi_4Mn_3O_{11.5}$ were prepared from the reaction between Bi_2O_3/BiOCl/PbO/MnO_2 (3:6:1:1) in a sealed gold tube during 12 h at 1173 K and slow cooling down to 973 K for 99 h. EDX analyzes of isolated triangular black platelike crystals

indicate the absence of Pb and Cl as constituting element. The determined Bi/Mn ratio is 8/5.3. The single crystal formula is $[Mn_{3+x}O_7][Bi_4O_{4.5-y}]$ with, $x = 0.03$ and $y = 0.15$. After a number of different attempts to produce this phase, we note the systematic predominance of $Bi_2Mn_4O_{10}$, which is thermodynamically stable as soon as the temperature reaches 823 K (Figure 4a–d). Only the decomposition at intermediate temperature of the product obtained by the Pechini method shows the appearing of the expected phase (Figure 4c). Typically, a bismuth citrate and manganese acetate mixture (8:6 ratio) was dissolved in a hot water using the minimum amount of ammonia and polymerized by citric acid and ethylene glycol in 4:1 ratio after evaporation. Organic species were removed first in air at 573 K, and then followed by in situ high-temperature XRD (Figure 4c,d). The compound was identified by its theoretical XRD pattern (Figure 4e), which shows evidence of the phase between 723 K and 773 K, and transforms into $Bi_2Mn_4O_{10}/\gamma$-Bi_2O_3 at higher temperature. A large amount of single-phase material was finally prepared using a long-time (3 days) decomposition of the original gel at 773 K.

Powder XRD was performed on Bruker D8 diffractometer, CuKα radiation. High temperature X-ray diffraction (HT-XRD) experiments were carried out from room-temperature up to 923 K using an Anton Paar HTK 1200N chamber under nitrogen flow. Single-crystal XRD data were collected using a Bruker Apex Duo diffractometer with a Mo-IμS microfocus tube ($\lambda = 0.71073$ Å) equipped with Oxford Cryostream 700 device. The crystal structure of $[Mn_{3+x}O_7][Bi_4O_{4.5-y}]$ was solved using the charge-flipping algorithm implemented in Superflip[10] and refined using Jana2006[11] (rhombohedral, space group $R\bar{3}$, $a = 7.7199(1)$ Å, $c = 27.8588(7)$ Å, $R_F = 1.96\,\%$, $wR_F = 2.59\,\%$ for $I > 3\sigma(I)$). Details of the data collection and refined parameters are given in the Supporting Information, S1. The intensity data have been extracted from the collected frames using the program SAINT-Plus 6.02.[25] The lattice parameters were defined from the complete data set. Absorption corrections were performed for both compounds using SADABS.[26]

Iodometric titration was used to determine the Mn oxidation state 0.02 g of the sample was dissolved in 40 mL 9.25% solution of HCl with an excess of KI under flowing nitrogen. The titration was performed by 0.01M solution of $Na_2S_2O_3$. Conductivity measurements were carried out on a homemade four-probe cell set in the DE-202 cryostat over the 30–330 K temperature range. Gold wires were fixed on a single crystals using graphite paste. Electron diffraction patterns were obtained on a FEI Technai G220 transmission electron microscope equipped with a precession system. The material was crushed and dispersed on a holey carbon film deposited on a Cu grid. Magnetic measurements were carried out on a MPMS SQUID-VSM (Quantum Design) magnetometer between 1.8 and 300 K at 0 to 7 T. The susceptibility versus temperature measurement was carried out under 0.1 Tesla after the sample was cooled in a field of 0.1 T (FC) or in zero field (ZFC). Previously, powders were magnetically aligned at 7 T in a polymeric gel that freezes the particle orientation below about 303 K.

Received: May 16, 2012
Published online: August 15, 2012

Keywords: bismuth · magnetism · manganese · maple-leaf lattices · solid-state structures

[1] A. J. Leggett, *Nat. Phys.* **2006**, *2*, 134–136.
[2] J. E. Greedan, N. P. Raju, A. S. Wills, C. Morin, S. M. Shaw, J. N. Reimers, *Chem. Mater.* **1998**, *10*, 3058–3067.
[3] A. Rolle, V. Thoréton, P. Rozier, E. Capoen, O. Mentré, B. Boukamp, S. Daviero-Minaud, *Fuel Cells* **2012**, *12*, 288–301.
[4] K. Nagasawa, S. Daviero-Minaud, N. Preux, A. Rolle, P. Roussel, H. Nakatsugawa, O. Mentré, *Chem. Mater.* **2009**, *21*, 4738–4745.
[5] S. Ishiwata, I. Terasaki, F. Ishii, N. Nagaosa, H. Mukuda, Y. Kitaoka, T. Saito, M. Takano, *Phys. Rev. Lett.* **2007**, *98*, 217201.
[6] L. E. De Long, L. Shlyk, G. Cao, *Proc. Int. Conf. Electromagnetics Adv. Appl.* **2009**, 929–932.
[7] M. Sturza, H. Kabbour, S. Daviero-Minaud, D. Filimonov, K. Pokholok, N. Tiercelin, F. Porcher, L. Aldon, O. Mentre, *J. Am. Chem. Soc.* **2011**, *133*, 10901–10909.
[8] J. Post, D. Appleman, *Am. Mineral.* **1988**, *73*, 1401–1404.
[9] J. Richter, J. Schulenburg, A. Honecker in *Quantum Magnetism* (Eds.: U. Schollwöck, J. Richter, D. Farnell, R. Bishop), Springer, Berlin, **2004**, pp. 85–153.
[10] L. Palatinus, G. Chapuis, *J. Appl. Crystallogr.* **2007**, *40*, 786–790.
[11] V. Petricek, M. Dusek, L. Palatinus, *Jana2006. The Crystallographic Computing System*, Institute Of Physics, Praha, Czech Republic, **2006**.
[12] S. V. Krivovichev, S. K. Filatov, T. F. Semenova, *Russ. Chem. Rev.* **1998**, *67*, 137–155.
[13] N. Cornei, N. Tancret, F. Abraham, O. Mentré, *Inorg. Chem.* **2006**, *45*, 4886–4888.
[14] A.-C. Gaillot, V. A. Drits, A. Manceau, B. Lanson, *Microporous Mesoporous Mater.* **2007**, *98*, 267–282.
[15] B. Toner, A. Manceau, S. M. Webb, G. Sposito, *Geochim. Cosmochim. Acta* **2006**, *70*, 27–43.
[16] K. D. Kwon, K. Refson, G. Sposito, *Geochim. Cosmochim. Acta* **2009**, *73*, 1273–1284.
[17] D. Schmalfuß, P. Tomczak, J. Schulenburg, J. Richter, *Phys. Rev. B* **2002**, *65*, 224405.
[18] T. Fennell, J. O. Piatek, R. A. Stephenson, G. J. Nilsen, H. M. Rønnow, *J. Phys. Condens. Matter* **2011**, *23*, 164201.
[19] D. Cave, F. C. Coomer, E. Molinos, H. Klauss, P. T. Wood, *Angew. Chem.* **2006**, *118*, 817–820; *Angew. Chem. Int. Ed.* **2006**, *45*, 803–806.
[20] N. Floros, C. Michel, M. Hervieu, B. Raveau, *J. Solid State Chem.* **2002**, *168*, 11–17.
[21] N. Henry, L. Burylo-Dhuime, F. Abraham, O. Mentre, *Solid State Sci.* **2002**, *4*, 1023–1029.
[22] L. Capriotti, A. E. Trumper, S. Sorella, *Phys. Rev. Lett.* **1999**, *82*, 3899–3902.
[23] H. T. Zhu, J. Luo, H. X. Yang, J. K. Liang, G. H. Rao, J. B. Li, Z. M. Du, *J. Phys. Chem. C* **2008**, *112*, 17089–17094.
[24] M. Drache, P. Roussel, J. Wignacourt, *Chem. Rev.* **2007**, *107*, 80–96.
[25] *SAINT: Area-Detector Integration Software*, Siemens Industrial Automation, Inc., Madison, **1996**.
[26] *SADABS: Area-Detector Absorption Correction*, Siemens Industrial Automation, Inc., Madison, **1995**.

